Characterization of a Mixed-Valence Ru(II)/Ru(III) Ion-Pair Complex. Unexpected High-Frequency Electron Paramagnetic Resonance Evidence for Ru(III)−Ru(III) Dimer Coupling

Olga Impert, Anna Kozakiewicz, Grzegorz Wrzeszcz, Anna Katafias, Alina Bieńko, Rudi van Eldik,* and Andrew Ozarowski*

ACCESS | 📊 Metrics & More | 📄 Article Recommendations | 🅢 Supporting Information

ABSTRACT: In this contribution, we report the synthesis and full characterization of the first mixed-valence Ru(II)/Ru(III) ion-pair complex, $[Ru^{II}(bipy)_2(pic)]^+[cis\text{-}Ru^{III}Cl_2(pic)_2]^-$, in the solid state and in aqueous solution, where bipy = 2,2′-bipyridine and pic^- = picolinate. In addition, unexpected high-frequency electron paramagnetic resonance evidence for interactions between two neighboring Ru(III) ions, resulting in a triplet state, $S = 1$, was found.

First Ru^{II}/Ru^{III} ion-pair complex!
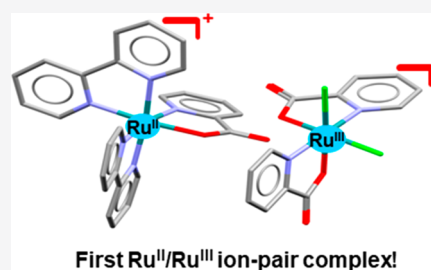
INTRODUCTION

The potential application of Ru(III) and Ru(II) complexes as anticancer, antiproliferative, and antimicrobial drugs is presently, being widely explored as outlined in a recent monograph on photochemical and biomedical applications of ruthenium complexes.[1] Promising drug candidates have been found within the diversity of families of ruthenium compounds developed, ranging from inorganic Ru(III) and Ru(II) octahedral complexes, to several types of organometallic Ru(II) compounds. According to common hypothesis, Ru(III) complexes are considered as potential drugs for the treatment of cancer usually activated by reduction.[2−4] However, the latter aspect has recently been critically discussed in a microreview by Alessio.[5] On the other hand, organometallic Ru(II) complexes are applied with great success in redox cell biology dealing with transfer hydrogenation, antiproliferative, and antimicrobial activity.[6−10] Is it possible to combine these properties in a mixed-valence Ru(II)/Ru(III) ion-pair complex that would have unique properties? This challenge forms the theme of the present report.

In the past, our mechanistic work focused on Ru(III) picolinate (pic) and Ru(II) polypyridyl complexes.[11−16] More recently, we initiated synthetic work to prepare complexes with mixed picolinate and polypyridyl ligands. Unfortunately, our synthetic efforts ended up in a mixture of unidentifiable complexes. Subsequently, we applied electrospray ionization mass spectrometry (ESI-MS) techniques to monitor the synthetic procedures and to guide the isolation of crystalline products. By coincidence, we succeeded in the isolation of a few crystals of the mixed-valence Ru(II)/Ru(III) ion-pair complex, $[Ru^{II}(bipy)_2(pic)]^+[cis\text{-}Ru^{III}Cl_2(pic)_2]^-$. To the best of our knowledge, such ion-pair complexes have not been

reported in the literature to date. This stands in contrast to numerous mixed-valence Ru(II)−Ru(III) bridged binuclear complexes that date back to the midseventies and the impressive work performed by Henry Taube and collaborators,[17,18] and more contemporary reports by Kaim, Lahiri, and others.[19,20] In order to perform a full characterization of the isolated ion-pair complex, significantly more material was required. We struggled for almost 18 months to repeat the synthesis in a reproducible manner, which was again guided by the application of ESI-MS spectroscopy. The isolated compound was fully characterized in the solid state and in solution. Such complexes in principle seem to have a unique potential in terms of the combined ability of the Ru(III) anionic complex to act as a drug in antitumor chemistry and of the Ru(II) cationic complex to be applied in redox cell biology.

EXPERIMENTAL SECTION

Materials. $RuCl_3 \cdot xH_2O$, 2-picolinic acid, and 2,2′-bipyridine were purchased from Sigma-Aldrich, and other reagents were from Avantor Performance Materials Poland SA. Doubly deionized water was used throughout all experiments. All chemicals were used without further purification.

Synthesis of $[Ru^{II}(bipy)_2(pic)]^+[cis\text{-}Ru^{III}Cl_2(pic)_2]^-$. $RuCl_3 \cdot xH_2O$ (502 mg, 1.92 mmol) dissolved in anhydrous ethyl alcohol (75 mL) was refluxed for 3 h. The reaction mixture was filtered while hot to
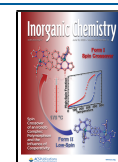
remove any undissolved material. Then, picolinic acid (239 mg, 1.94 mmol) and bipyridine (600 mg, 3.84 mmol) were added to the solution and refluxed further under argon atmosphere. After 1.5 h, a reddish brown powder precipitated. Refluxing was continued for 8 h, and the powder was filtered off. A small quantity of brown crystals (4 mg) was obtained from the filtrate after a period of four months.

To prepare a larger amount of sample of the mixed-valence Ru(II)/Ru(III) ion-pair, a more efficient method had to be worked out. The ion-pair was synthesized by mixing equimolar amounts of $H_2pic[cis-Ru^{III}Cl_2(pic)_2]\cdot1.5H_2O$ and $[Ru^{II}(bipy)_2(pic)]Cl\cdot5.5H_2O$ in ethanol−water (1:1) solution of pH 3.60 adjusted by HCl. Yield: 24 mg (56%). Elemental analysis calculated for $C_{38}H_{28}Cl_2Ru_2N_7O_6$ (951.71 g mol^{-1}): C 47.96, H 2.97, N 10.14; found C 47.90, H 3.04, N 10.14. IR (cm^{-1}): 3082w, 1651sh, 1628s, 1596s, 1460m, 1439m, 1346m, 1309m, 1272m, 1244m, 1147w, 1013w, 850m, 760s, 729m, 713m, 691s, 658m, 545w, 470m, 457m, 429w, 341s, 322sh, 280m, 253m, 236w, 214w, 195w, 150w, 141w, 126w. UV−vis λ_{max}, nm (ε, M^{-1} cm^{-1}): 254 (32370), 289 (55270), 470 (10460).

$H_2pic[cis-Ru^{III}Cl_2(pic)_2]$ was prepared according to a procedure reported by us before.[12] $[Ru^{II}(bipy)_2(pic)]Cl\cdot5.5H_2O$ was synthesized using a slight modification of the synthesis described in the literature (for further details on the structure of this complex, see Supporting Information, Figure S1 and Tables S1−S3).[21] $[Ru(bipy)_2Cl_2]\cdot2H_2O$[22] (52 mg, 0.1 mmol) dissolved in water (5 mL) was refluxed for 1 h under an argon atmosphere. Then picolinic acid (13.7 mg, 0.1 mmol) dissolved in ethanol (5 mL) was added, and the reaction mixture was refluxed for further 4 h. The obtained solution was evaporated under argon to dryness, and the solid was dissolved in water (18 mL). The volume of the orange-red solution was reduced to one-third in a stream of cold air. The orange crystals were collected by filtration and washed with ether. Yield: 26.7 mg (47%).

■ METHODS

Powder diffraction experiments were performed with a PANalytical X'Pert PRO MPD diffractometer equipped with a copper X-ray tube with operating conditions of 40 kV and 30 mA. The sample was powdered using an agate mortar and transferred onto a zero-background, silicon flat plate holder. The measurement was done in Bragg−Brentano geometry (flat plate reflection) with fixed slit sizes. A graphite crystal X-ray monochromator (oriented with 002 plane) was used on the diffracted beam to remove Kβ radiation.

A Quanta field-emission gun scanning electron microscope (SEM; Quanta 3D FEG; Carl Zeiss, Göttingen, Germany) was used to generate images of the mixed-valence ion-pair crystals shown in Figure S2 (Supporting Information).

Energy-dispersive X-ray spectroscopy (EDX) analysis was performed with a scanning electron microscope (SEM, Zeiss, Leo 1430 VP, Carl Zeiss, Oberkochen, Germany) coupled to an energy-dispersive X-ray fluorescence spectrometer (EDX) Quantax 200 with the XFlash 4010 (Bruker AXS, Karlsruhe, Germany) detector.

IR spectrum was recorded with a Bruker-Optics Vertex 70v FTIR spectrometer with ATR optics (diamond crystal) in the 4000−30 cm^{-1} range.

Magnetic susceptibility was measured at room temperature by the Faraday method with a balance constructed in our laboratory at a field strength up to 1.0 T. The magnetic field was calibrated with Hg[Co(NCS)$_4$].[23] The molar susceptibility was corrected for diamagnetism using Pascal's constants.[24]

Magnetic measurements. Magnetic data were collected, using a Quantum Design MPMS-XL-5 SQUID magnetometer, calibrated with a palladium rod (Materials Research Corporation, purity 99.9985%). The superconducting magnet operated at a field from 0 to 50 kOe. Magnetic susceptibility data were collected over the temperature range 1.8−300 K and an applied magnetic field of 0.5 T. Magnetization data were measured using a magnetic field from 0 to 50 kOe at 2 K. The raw data were corrected for background signals and for the underlying diamagnetism, calculated from Pascal's constants.[24]

An EPR spectrum of a powdered sample was recorded at room temperature with an X band (ca. 9.33 GHz) Radiopan EPR SE/X-2541 M spectrometer with a 100 kHz modulation. The microwave frequency was monitored with a frequency meter. The magnetic field was measured with an automatic NMR-type JTM-147 magnetometer. X-band EPR spectrum of a frozen solution (water/ethanol/ethylene glycol) of $[Ru(bipy)_2(pic)]^+[cis-RuCl_2(pic)_2]^-$ was measured at 77 K using a Bruker ELEXYS E500 spectrometer equipped with a NMR teslameter and frequency counter. The experimental spectrum was simulated with the DoubletExact ($S = 1/2$) computer program.[25] High-frequency EPR spectra were recorded at temperatures 3−100 K with a home-built spectrometer at the EMR facility of NHMFL. The instrument is a transmission-type device (using no resonance cavity) in which waves propagate in cylindrical light-pipes. The microwave source consisted of a phase-locked oscillator (Virginia Diodes) operating at an adjustable basic frequency of 8−20 GHz and a frequency multiplier chain generating its harmonics, of which the 4th, 8th, 12th, 16th, 24th, and 32nd were available. A superconducting magnet (Oxford Instruments) capable of reaching a field of 17 T was employed.[26]

^{1}H NMR spectra were recorded on Bruker Avance-400 and Bruker Avance-700 NMR spectrometers. ^{1}H shifts were referenced to TMS.

ESI-MS spectra were recorded using a Bruker MicrOTOF-Q II instrument with 4.5 kV capillary voltage and dry gas flow (N$_2$) of 4 L/min. Samples of the complex dissolved in ultrapure water were injected into the ESI-MS-TOF chamber calibrated according to the manufacturer's procedure (clusters of 10 mM sodium formate in a 2-propanol/water mixture (1:1, v/v)). The flow rate was set at 3 μL/min. The MS measurements were performed in the positive and negative ion modes, and the selected range was from 50 to 3000 m/z.

Electronic spectra were recorded on a Shimadzu UV-1601 PC spectrophotometer thermostated with a Julabo F25 cryostat.

X-ray Crystallography. The brown block crystals of $[Ru^{II}(bipy)_2(pic)]^+[cis-Ru^{III}Cl_2(pic)_2]^-$ were obtained directly from the reaction mixture. The X-ray data for the reported structure were collected at 293(2) K with an Oxford Sapphire CCD diffractometer using Mo Kα radiation λ = 0.71073 Å and the ω-2θ method. The structure was solved by direct methods and refined with the full-matrix least-squares method on F^2 with the use of the SHELX2014 program packages.[27] Analytical absorption corrections were applied (CrysAlis version 171.38.43 package of programs[28] Rigaku OD, 2015). Positions of hydrogen atoms were found from the electron density maps, and hydrogen atoms were constrained during refinement with the appropriate riding model as implemented in SHELX during refinement. The data collection and refinement processes are summarized in Table 1, and selected bond lengths and angles are presented in Table 2. The structural data have been deposited at the Cambridge Crystallographic Data Centre: CCDC No 1857947.

■ RESULTS AND DISCUSSION

The mixed-valence Ru(II)/Ru(III) ion-pair complex $[Ru^{II}(bipy)_2(pic)]^+[cis-Ru^{III}Cl_2(pic)_2]^-$, crystallized in the monoclinic crystal system (space group $P2_1/c$). X-ray analysis showed that in the asymmetric unit, the Ru(II) ion with one picolinate and two 2,2′-bipyridine ligands, as well as the Ru(III) ion with two picolinate ligands and two Cl$^-$ ions, are present (Figure 1). Both Ru ions are six-coordinate in the deformed octahedral geometry. The coordination sphere of Ru(II) consists of two N atoms of two 2,2′-bipyridine ligands (N1, N12, N13, and N24), and N and O atoms of the picolinate ligand (N25, O33), with N12 and N25 atoms in the trans positions. While the coordination sphere of Ru(III) is formed by two bidentate picolinate ligands and two Cl$^-$ ions, the N40 and N57 atoms are positioned trans to each other. Oxygen atoms of carboxyl groups (O49 and O48) are in the cis position.

For $[Ru^{II}(bipy)_2(pic)]^+$, two 2,2′-bipyridine ligands are situated almost perpendicular with a dihedral angle, measured
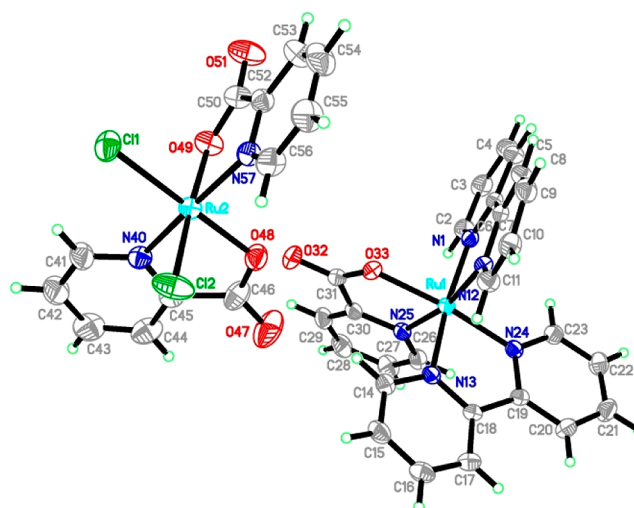
Table 1. Crystal Data and Structure Refinement Parameters for $[Ru^{II}(bipy)_2(pic)]^+[cis\text{-}Ru^{III}Cl_2(pic)_2]^-$

identification code	$[Ru^{II}(bipy)_2(pic)]^+[cis\text{-}Ru^{III}Cl_2(pic)_2]^-$
CCDC	1857947
empirical formula	$C_{38}H_{28}Cl_2Ru_2N_7O_6$
formula weight. g mol^{-1}	951.71
crystal size, mm	$0.285 \times 0.202 \times 0.190$
crystal system	monoclinic
space group	$P2_1/c$
a, Å	14.2862(8)
b, Å	13.1875(7)
c, Å	20.0961(10)
β, deg	100.469(5)
volume, Å^3	3723.1(3)
Z	4
density (calc), g cm^{-3}	1.698
absorption coefficient, mm^{-1}	1.012
$F(000)$	1904
θ range, deg	2.118–28.591
reflections collected/unique	27014/8589 [R(int) = 0.0497]
index ranges hkl	$-15 \leq h \leq 19, -17 \leq k \leq 15, -26 \leq l \leq 25$
restraints/parameters	0/496
goodness of fit on F^2	1.040
final R indices [$I > 2\sigma(I)$]	$R_1 = 0.0345, wR_2 = 0.0753$
R indices (all data)	$R_1 = 0.0525, wR_2 = 0.0831$
max electron density/e·Å^{-3}	0.560
min electron density/e·Å^{-3}	-0.580

Table 2. Selected Bond Lengths [Å] and Angles [°] for $[Ru^{II}(bipy)_2(pic)]^+[cis\text{-}Ru^{III}Cl_2(pic)_2]^-$

Bond Lengths [Å]			
Ru1−N1	2.064(2)	Ru2−N40	2.056(3)
Ru1−N12	2.047(2)	Ru2−N57	2.058(2)
Ru1−N13	2.048(2)	Ru2−O48	2.036(2)
Ru1−N24	2.044(2)	Ru2−O49	2.021(2)
Ru1−N25	2.059(2)	Ru2−Cl1	2.3405(9)
Ru1−O33	2.088(2)	Ru2−Cl2	2.3308(8)
Angles [deg]			
N24−Ru1−N12	91.36(9)	O49−Ru2−O48	87.35(9)
N24−Ru1−N13	79.32(8)	O49−Ru2−N40	95.49(9)
N12−Ru1−N13	93.63(9)	O48−Ru2−N40	80.41(10)
N24−Ru1−N25	99.20(9)	O49−Ru2−N57	80.04(9)
N12−Ru1−N25	168.08(9)	O48−Ru2−N57	96.01(9)
N13−Ru1−N25	93.74(9)	N40−Ru2−N57	174.45(9)
N24−Ru1−N1	96.74(8)	O49−Ru2−Cl2	175.81(7)
N12−Ru1−N1	79.21(9)	O48−Ru2−Cl2	91.45(7)
N13−Ru1−N1	171.81(9)	N40−Ru2−Cl2	88.26(7)
N25−Ru1−N1	93.99(9)	N57−Ru2−Cl2	96.10(7)
N24−Ru1−O33	173.35(8)	O49−Ru2−Cl1	88.73(7)
N12−Ru1−O33	91.21(8)	O48−Ru2−Cl1	174.70(7)
N13−Ru1−O33	94.40(8)	N40−Ru2−Cl1	96.42(7)
N25−Ru1−O33	78.89(9)	N57−Ru2−Cl1	86.82(7)
N1−Ru1−O33	89.77(8)	Cl2−Ru2−Cl1	92.70(4)

Figure 1. Crystal structure of $[Ru^{II}(bipy)_2(pic)]^+[cis\text{-}Ru^{III}Cl_2(pic)_2]^-$ with the thermal ellipsoids plotted at 30% probability.

Analysis of crystal packing in $[Ru^{II}(bipy)_2(pic)]^+[cis\text{-}Ru^{III}Cl_2(pic)_2]^-$ (Figure 2) revealed intra- and intermolecular
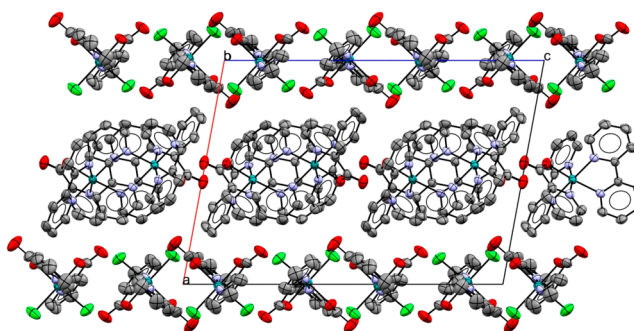
Figure 2. Crystal packing of the mixed-valence Ru(II)/Ru(III) ion-pair complex along the b axis revealing layers of $[Ru^{II}(bipy)_2(pic)]^+$ cations and $cis\text{-}[Ru^{III}Cl_2(pic)_2]^-$ anions arranged alternately.

C−H···X (X = N, O, Cl) interactions (Table 3). In this structure, intermolecular interactions C−H···O between two complex ions $cis\text{-}[Ru^{III}Cl_2(pic)_2]^-$ were found, with C55−H55A···O47 $[-x + 2, -y + 2, -z + 1]$ and C55−H55A···O48 $[-x + 2, -y + 2, -z + 1]$ distances of 2.580 and 2.621 Å, respectively. Further structural information is given in Figures S2−S4 in Supporting Information.

$\pi−\pi$ Interactions. The distance between the ring gravity centers (see below) is slightly above 4 Å (a critical value), whereas the Ru(III)−Ru(III) distance is 8.699 Å (Figure 3). Intermolecular $\pi···\pi$ interactions between the Ru(III) units are detected between 6-membered rings of two picolinate ligands, with $\pi_{[N40\cdot\cdot C41]}···\pi_{[N40−C41]}$ $[2 - x, 1 - y, 1 - z]$ distance between the ring gravity centers and slippage being 4.109(2) and 1.881 Å, respectively. The six-membered ring planes are perfectly parallel with the dihedral angle being 0°.

A search in the CSD database[29] revealed that no similar mixed-valence Ru(II)/Ru(III) ion-pair complex of the structure described here could be found. There are only two entries containing $[Ru^{II}(bipy)_2(pic)]^+$, but with different simple counterions, such as Cl$^-$ and PF$_6^-$.[21,30] Also, only four structures with the same $[cis\text{-}Ru^{III}Cl_2(pic)_2]^-$ anion were found in the CSD database.[12,13]

between best planes of these two rings, of 87.7(3)°. An almost perpendicular mutual position of the picolinate ligand and two 2,2′-bipyridine ligands is also observed. The dihedral angles between the best planes of these two rings are 84.8(4) and 78.1(3)°. For $cis\text{-}[Ru^{III}Cl_2(pic)_2]^-$ two picolinate ligands are situated almost perpendicular with a dihedral angle of 85.6(3)°.

Table 3. Intra- and Intermolecular Interactions in $[Ru^{II}(bipy)_2(pic)]^+[cis\text{-}Ru^{III}Cl_2(pic)_2]^-$

D−H···A	d(D−H)	d(H···A)	∠DHA	d(D···A)
C2−H2A···N25	0.930	2.672	115.84	3.189
C3−H3A···Cl2 [$x − 1, y, z$]	0.930	2.989	132.78	3.684
C5−H5A···O33 [$−x + 1, −y + 2, −z + 1$]	0.930	2.529	141.29	3.306
C8−H8A···O32 [$−x +1, −y + 2, −z + 1$]	0.930	2.621	154.08	3.482
C8−H8A···O33 [$−x +1, −y + 2, −z + 1$]	0.930	2.540	151.78	3.388
C11−H11A···N13	0.930	2.602	117.01	3.136
C14−H14A···O33	0.930	2.594	118.49	3.145
C15−H15A···O51 [$x, −y + 3/2, z − 1/2$]	0.930	2.583	122.30	3.178
C17−H17A···O32 [$x, −y + 3/2, z − 1/2$]	0.930	2.625	175.08	3.552
C20−H20A···O32 [$x, − y + 3/2, z − 1/2$]	0.930	2.473	171.40	3.396
C23−H23A···O51 [$-x+1, -y+2, -z+1$]	0.930	2.533	135.64	3.263
C26−H26A···Cl1 [$x − 1, −y + 3/2, z − 1/2$]	0.930	2.803	117.77	3.340
C29−H29A···O32 [$−x + 1, −y + 1, −z + 1$]	0.930	2.472	141.22	3.250
C41−H41A···Cl1	0.930	2.813	121.75	3.395
C43−H43A···Cl2 [$1 − x, 1 − y, 1 − z$]	0.930	2.767	135.15	3.489
C53−H53A···Cl1 [$−x + 2, y + 1/2, −z + 3/2$]	0.930	2.852	152.90	3.705
C55−H55A···O47 [$−x + 2, −y + 2, −z + 1$]	0.930	2.580	145.05	3.384
C55−H55A···O48 [$−x + 2, −y + 2, −z + 1$]	0.930	2.621	117.44	3.159
C56−H56A···Cl2	0.930	2.823	120.32	3.389
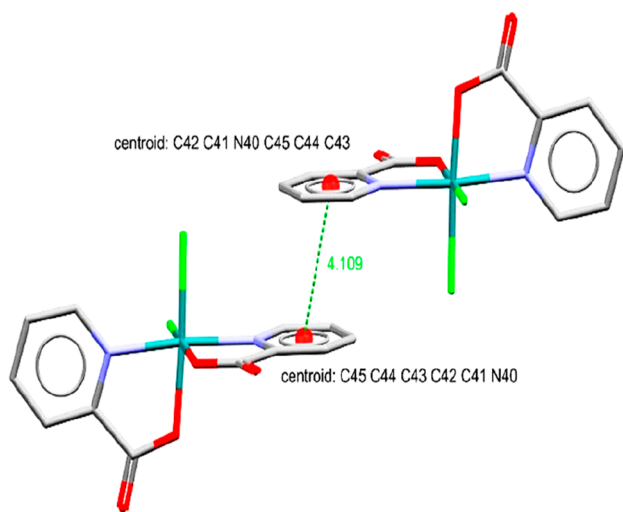
Figure 3. Unique $\pi\cdots\pi$ interactions between cis-$[Ru^{III}Cl_2(pic)_2]^-$ anions giving $S = 1$.

The following analyses were performed to check the homogeneity and purity of the bulk material. The X-ray powder diffraction pattern was measured and compared with the pattern calculated from the X-ray single-crystal data. Figure 4 and Table S4 (Supporting Information) show a very good agreement between experimental and calculated diffraction patterns. Differences in the peak intensities originate from a small quantity of available sample and preferred orientation

effects introduced in sample preparation for a flat-plate reflection measurement.

Elemental composition of the $[Ru^{II}(bipy)_2(pic)]^+[cis\text{-}Ru^{III}Cl_2(pic)_2]^-$ ion-pair complex was studied by the EDX method. Samples were taken from different batches of the product obtained. A typical EDX spectrum is presented in Figure 5. The lack of any signals corresponding to elements other than expected for the $[Ru^{II}(bipy)_2(pic)]^+[cis\text{-}Ru^{III}Cl_2(pic)_2]^-$ ion-pair complex indicates that the obtained sample is free of any impurities. Aluminum detected in the analysis originates from the microscope table.

The IR spectrum of the solid $[Ru^{II}(bipy)_2(pic)]^+[cis\text{-}RuCl_2(pic)_2]^-$ ion-pair complex (see Figure S6, Supporting Information) obviously presents the characteristic absorptions of both the coordinated picolinate anion and bipyridine, and the metal−ligand bonds. Because of the presence of both Ru(II) and Ru(III) complex ions, the IR spectrum is complicated, showing many bands (see Experimental Section), and only tentative assignments, based on literature data, are given below.[31−34] The characteristic sharp and strong or medium bands at 1651, 1460, 1272, 1244, 850, 760, 691, 470 cm^{-1} are consistent, within the experimental error, with literature data for both mer-$[Ru(pic)_3]$[33,34] and $[H(Hpic)_2]$-$[cis\text{-}RuCl_2(pic)_2]\cdot2H_2O$,[13] therefore derived from the vibrations of a coordinated picolinate anion. The antisymmetric and symmetric stretching vibrations of carboxylate ions are observed at 1628 and 1309 cm^{-1}, respectively, with a $\nu_{as}−\nu_s$ separation of 319 cm^{-1}, i.e., much larger than in sodium picolinate, indicating the monodentate linkage of the carboxylate groups in the picolinate anion.[33,35,36]

The strong band at 1596 cm^{-1} corresponds to the pyridine-ring vibration. The increase in the value of the ring vibration (ca. 28 cm^{-1}) from the free ligand shows the coordination of the ring nitrogen to Ru(III). The weak bands observed in the 3100−2850 cm^{-1} range can be assigned to ν(CH) vibrations of both the pyridine ring.[37,38]

ESI-MS measurements were performed to identify the nature of the mixed-valence ion-pair in aqueous solution. The recorded spectra along with the spectra simulated using an open-source software[39] for the suggested species are shown in Figure 6. The spectra exhibit only two intense peaks at $m/z =$ 536.07 (positive mode) and 415.88 (negative mode) that are attributed to the $[Ru^{II}(bipy)_2(pic)]^+$ and cis-$[Ru^{III}Cl_2(pic)_2]^-$ species, respectively. The characteristic multiline patterns are due to various isotopes centered around $m/z = 536$ and 416 for Ru(II) and Ru(III) species, respectively. In both cases, spectral simulations for the suggested complex species agreed exactly with the experimental data.

The ^{1}H NMR spectrum of the obtained $[Ru^{II}(bipy)_2(pic)]^+$-$[cis\text{-}Ru^{III}Cl_2(pic)_2]^-$ ion-pair recorded in CD$_3$OD is fully consistent with its nature as revealed by X-ray diffraction and ESI-MS analyses, and confirms the presence of two ionic species (Figure S7a, Supporting Information). The proton signals of the diamagnetic $[Ru^{II}(bipy)_2(pic)]^+$ complex are observed within the 7.3−8.8 ppm range. Signals reported in the literature for $[Ru^{II}(bipy)_2(pic)]PF_6$[40] and $[Ru^{II}(bipy)_2(pic)]$-Cl[21] appeared within the same chemical shift range. The total integration corresponds to 20 protons, which is in agreement with the total number of protons in the diamagnetic cationic species (Figure S7a). Because of the presence of the paramagnetic cis-$[Ru^{III}Cl_2(pic)_2]^-$ complex, the proton signals are slightly broadened, resulting in a partial overlap of some of them, and splitting patterns different from those observed for
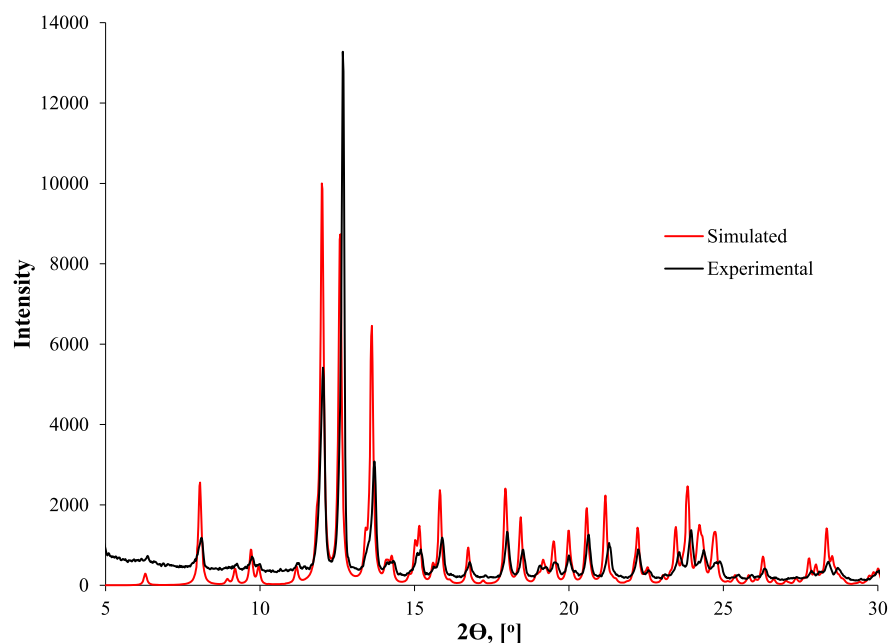
Figure 4. X-ray powder diffractogram of $[Ru^{II}(bipy)_2(pic)]^+[cis\text{-}Ru^{III}Cl_2(pic)_2]^-$.
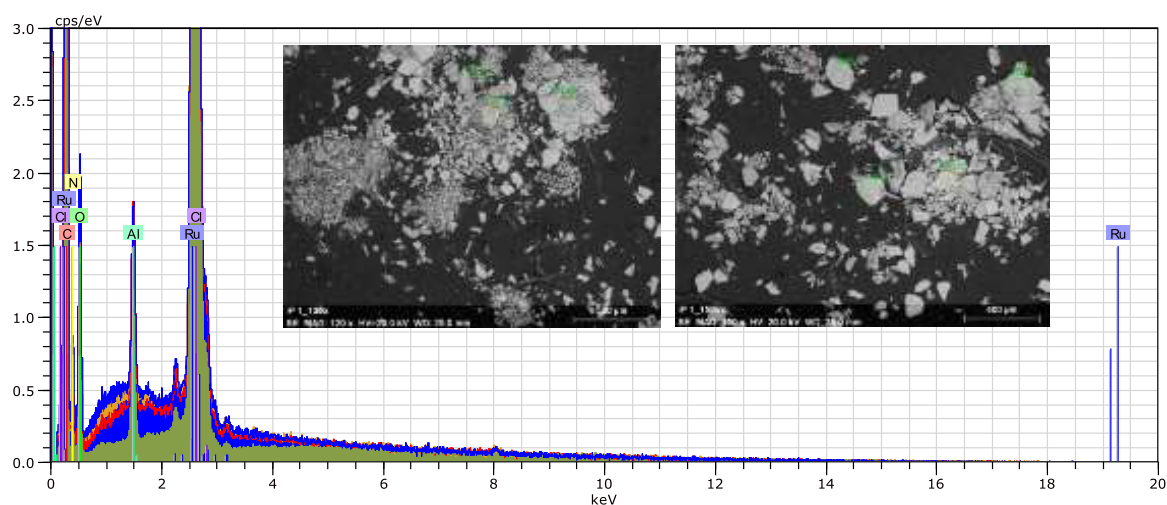
Figure 5. EDX spectrum with related SEM images of $[Ru^{II}(bipy)_2(pic)]^+[cis\text{-}Ru^{III}Cl_2(pic)_2]^-$.

the $[Ru^{II}(bipy)_2(pic)]Cl$ complex (Figure S7b). The paramagnetic $cis\text{-}[Ru^{III}Cl_2(pic)_2]^-$ complex gives four broad signals without splitting into multiplets at −4.74, −0.18, 0.90, and 9.93 ppm (Figure S7a), which are consistent with the chemical shifts observed in the ^1H NMR spectrum of the $H_2pic[cis\text{-}Ru^{III}Cl_2(pic)_2]$ complex (Figure S7c).

Electronic spectra of aqueous solutions of the mixed-valence $[Ru^{II}(bipy)_2(pic)]^+[cis\text{-}Ru^{III}Cl_2(pic)_2]^-$ ion-pair, $[Ru^{II}(bipy)_2(pic)]^+$, and $cis\text{-}[Ru^{III}Cl_2(pic)_2]^-$ ions are presented in Figure 7. The sum of the spectra of the cationic and anionic components of the ion-pair reproduces satisfactorily the experimental spectrum obtained for the ion-pair complex.

Magnetic Data. The $[Ru^{II}(bipy)_2(pic)]^+[cis\text{-}Ru^{III}Cl_2(pic)_2]^-$ complex at room temperature has an effective magnetic moment of 2.05 μ_B (measured by the Faraday method), which is typical for a single-unpaired-electron system. The value is consistent with the presence of diamagnetic d^6 Ru(II) and low-spin paramagnetic d^5 Ru(III), where the orbital degenerate $^2T_{2g}$ (O_h) ground state is split,

due to low symmetry ligand-field effects and spin−orbit coupling.

The thermal dependence of molar magnetic susceptibility (Figure 8) and the variation of magnetization versus magnetic field at 2 K (Figure 9) for $[Ru^{II}(bipy)_2(pic)]^+[cis\text{-}Ru^{III}Cl_2(pic)_2]^-$ were studied using SQUID magnetometer. At room temperature (300 K), the χT was equal to 0.831 $cm^3\cdot K\cdot mol^{-1}$, and it is strongly above 0.454 $cm^3\cdot K\cdot mol^{-1}$ calculated for the uncoupled ruthenium(III) ion ($S = 1/2$; $g = 2.2$). Then, a continuous almost linear drop to 0.489 $cm^3\cdot K\cdot mol^{-1}$ at 5 K was observed, succeeded by a further stronger decline to 0.478 $cm^3\cdot K\cdot mol^{-1}$ at 1.8 K. Such behavior clearly indicates a temperature independent paramagnetic (TIP) contribution to the magnetic susceptibility.

The M (μ_0H) plot (Figure 9) shows linear relation to ca. 10 kOe, then continues the Brillouin function and clearly indicates the ground spin state $S = 1/2$ with a value of M ca. 1.08 Mβ in the field 50 kOe. We used the PHI program, which allows for the simultaneous fitting of $\chi T(T)$ and $M(\mu_0H)$ dependences.[41]
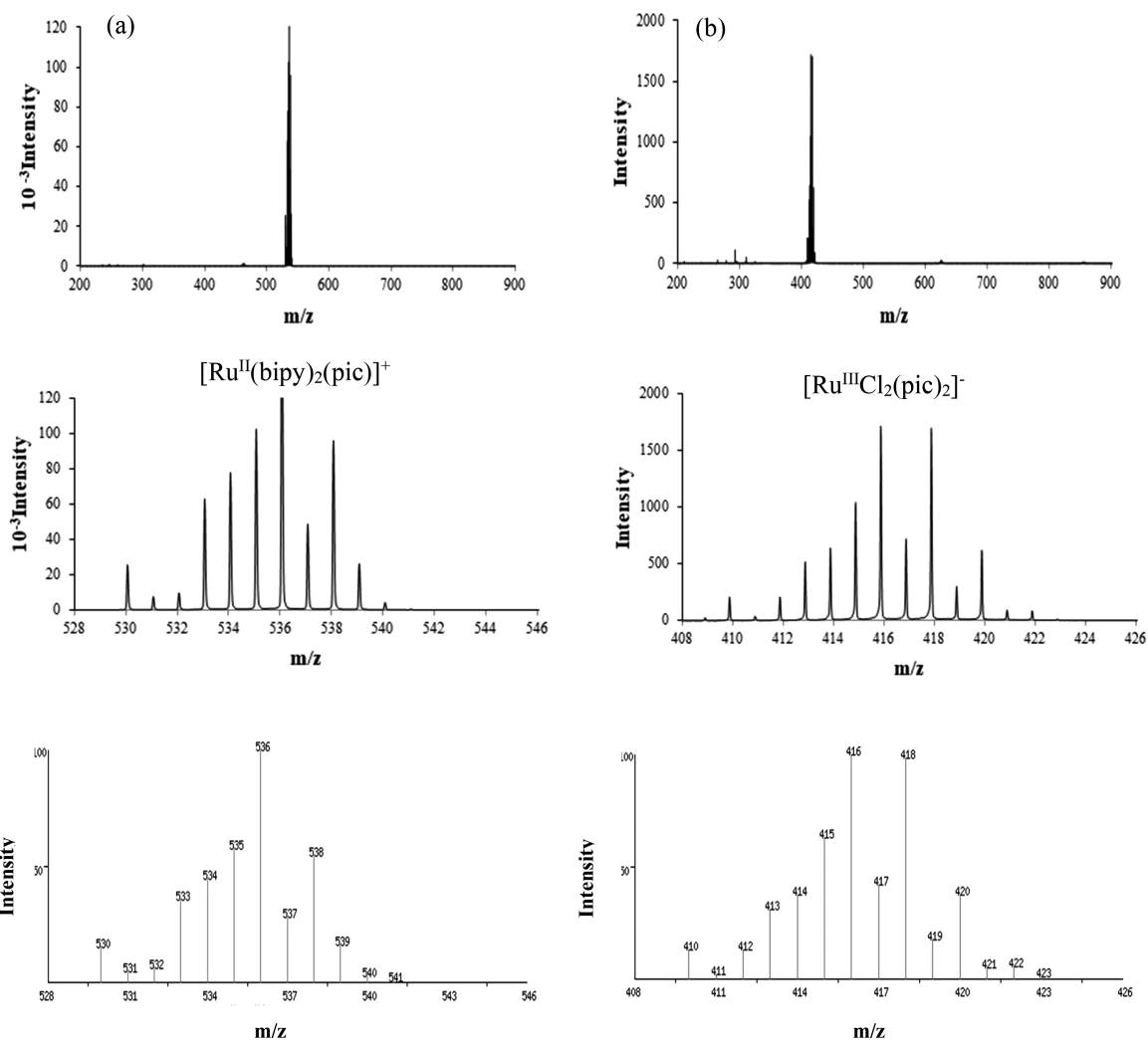
Figure 6. Experimental (top and middle) and simulated (bottom) ESI-MS spectra of $[Ru^{II}(bipy)_2(pic)]^+[cis\text{-}Ru^{III}Cl_2(pic)_2]^-$ dissolved in water, recorded in positive (a) and negative modes (b).
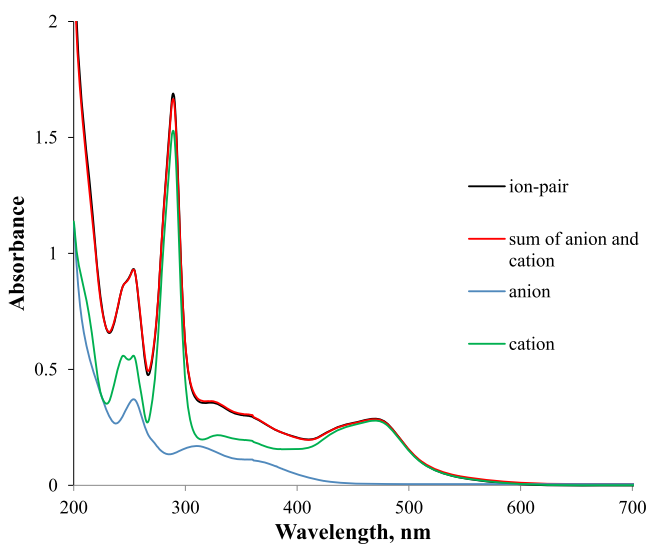
**Figure 7.** UV−vis absorption spectra of the mixed-valence $[Ru^{II}(bipy)_2(pic)]^+[cis\text{-}Ru^{III}Cl_2(pic)_2]^-$ ion-pair complex, $[Ru^{II}(bipy)_2(pic)]^+$ and $cis\text{-}[Ru^{III}Cl_2(pic)_2]^-$ ions, and the sum of the spectra of the cationic and anionic species; $[Ru^{II/III}] = 2.5 \times 10^{-5}$ M.
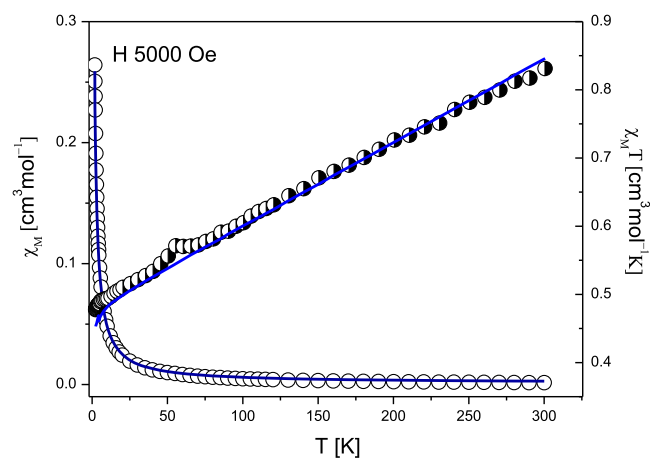
Figure 8. Thermal dependence of χ_M (open circle) and $\chi_M T$ product (half-filled circle) for $[Ru(bipy)_2(pic)]^+[cis\text{-}RuCl_2(pic)_2]^-$. The solid line is the calculated best fitted curve with the parameters given in the text.

The best reasonable fit (without points 50−60 K due to oxygen contamination) parameters was $g = 2.261$, TIP = 1.21 $\times 10^{-3}$ cm^3 mol^{-1} and molecular field correction $zJ' = 0.012$
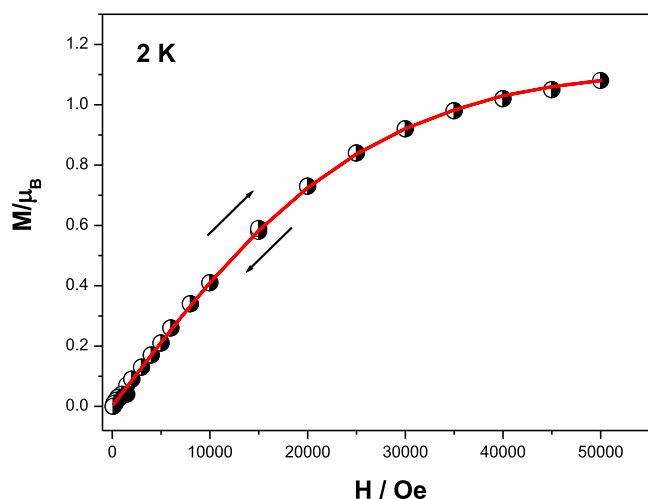
Figure 9. Field dependence of the magnetization for the [Ru-(bipy)$_2$(pic)]$^+$[cis-RuCl$_2$(pic)$_2$]$^-$ complex at 2 K. Line fitted using parameters given in the text.

cm^{-1} (Figure 9). It should be taken into account that parameters may compete with each other during the fitting procedure, leaving some degree of uncertainty, not only with the value, but also the nature of the zJ′ interactions.

The room temperature EPR spectrum of the [Ru^{II}(bipy)$_2$(pic)]$^+$[cis-Ru^{III}Cl$_2$(pic)$_2$]$^-$ mixed-valence ion-pair is rather unusual (Figure 10). In the middle- and high-
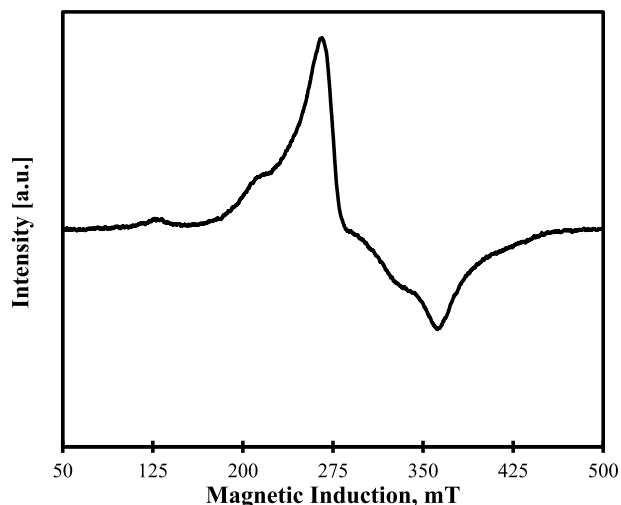
Figure 10. X-band (9.33037 GHz) EPR spectrum of powdered [Ru(bipy)$_2$(pic)]$^+$[cis-RuCl$_2$(pic)$_2$]$^-$ at room temperature.

field part, it exhibits distinct resonances which seem to be characteristic for the S = 1/2 spin system. The rhombic nature of this part of the spectrum indicates asymmetry of the electronic environment around Ru(III). The data are in accordance with the Ru(III) ion present in the distorted-octahedral ligand environment observed in the crystal structure. In principle, the EPR spectra and parameters for the cis-[RuCl$_2$(pic)$_2$]$^-$ species should be similar independent of the accompanying counterion, i.e., the [Ru^{II}(bipy)$_2$(pic)]$^+$ or [H(Hpic)$_2$]$^+$ cations.[12] However, this is not the case.

Moreover, the EPR spectrum (Figure 10) shows two additional signals of lower intensity at the low-field part with g-factors of ca. 5.2 and 3.1, which cannot be explained in an S =

1/2 system. Additional signals in EPR spectra of ruthenium-(III) complexes are occasionally reported in the literature, but their origin is either not explained as for [Ru(dipc)-(AsPh$_3$)$_2$Br] (H$_2$dipic-dipicolinic acid)[42] and [RuCl$_3$(dppb)-(DMSO)] (dppb - 1,4-bis(diphenylphosphino)butane)[19] or is admittedly related to the exchange interactions between two ruthenium(III) centers as for [RuCl$_3$(dppb)(H$_2$O)],[43] but without providing details. On the other hand, the EPR of a frozen solution of [Ru(bipy)$_2$(pic)]$^+$[cis-RuCl$_2$(pic)$_2$]$^-$ at 77 K shows a typical rhombic spectrum according to S = 1/2 spin Hamiltonian in the absence of hyperfine interactions. The best fit of the spectrum[25] was obtained with g$_x$ = 1.67, g$_y$ = 2.44, and g$_z$ = 2.56 (Figure 11).
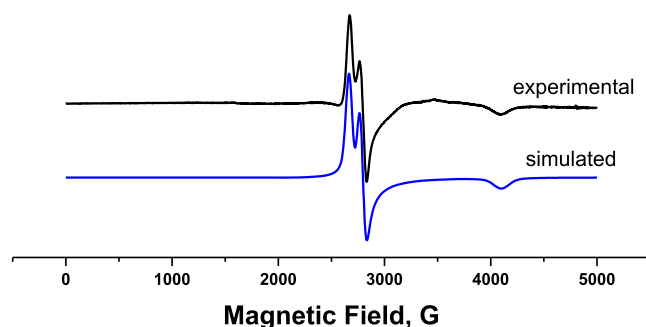

Figure 11. X-band (9.578417 GHz) EPR spectrum (experimental—black, simulated—blue) of a frozen solution (water/ethanol/ethylene glycol) of [Ru(bipy)$_2$(pic)]$^+$[cis-RuCl$_2$(pic)$_2$]$^-$ at 77 K.

Solid-state high-field EPR spectra were thus recorded to get a better insight into the system nature. Rhombic spectra with three very different g values, 2.533, 2.440 and 1.705, were seen (Figures 12 and 13). More interestingly, the feature
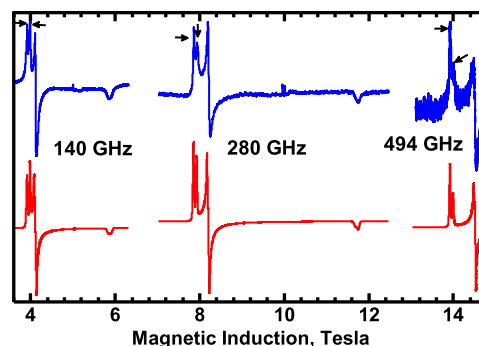
Figure 12. EPR spectra recorded at 30 K with microwave frequencies shown. Blue: experimental; red: simulated as explained in the text. The arrows point to the two components of the g = 2.533 feature. The splitting between them is frequency-independent.

corresponding to the largest g value was split into two components, separated by approximately 700 G over a frequency range of 140−500 GHz. The lack of dependence of this splitting on the microwave frequency indicates that it is not due to two slightly different g values, as in such case the splitting would be proportional to frequency. The higher-field component of that pattern can be "frozen out" when recording spectra at sufficiently low temperatures (Figure 13). The feature at g = 1.705 also appears to consist of two components. The splitting between them is smaller than seen in the g = 2.533 feature, and they are not clearly resolved. At sufficiently
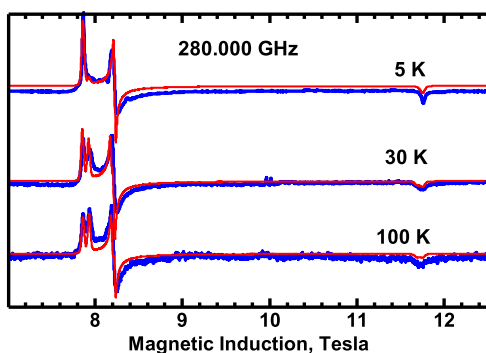
Figure 13. Temperature dependence of the 280 GHz spectra. Blue: experimental; red: simulated as explained in the text. At sufficiently low temperature, the higher-field component of the g = 2.533 feature and the lower-field component of the g = 1.705 disappear.

low temperature, only the higher-field component of that pair is seen. This behavior is consistent with a model of a $S = 1$ system resulting from the interactions between two $S = 1/2$ Ru(III) ions.

We have attempted to simulate our EPR spectra using the standard spin Hamiltonian for the $S = 1$ state.

$$\hat{H} = \mu_B B\{g\}\hat{S} + D\left\{\hat{S}_z^2 - \frac{1}{3}S(S+1)\right\} + E(\hat{S}_x^2 - \hat{S}_y^2)$$
(4)

For the purpose of discussing the zero-field splitting, it is convenient to label the g value on which the largest splitting is observed as g_z. The simulation procedures allowed to find $g_x = 2.440$, $g_y = 1.705$, $g_z = 2.533$, $D = -0.051$ cm^{-1}, $E = 0$. Assumption of the zero-field splitting tensor being rotated versus the g matrix by 20 deg about the Y axis improved the agreement between the simulated and experimental spectra, but it is not required to generate the splitting under discussion. Determination of the sign of D is straightforward in HF EPR, and negative D is consistent with "freezing out" of the higher-field component of the double line feature seen in Figure 7 at ~7.9 T. This effect is related to the magnitude of the Zeeman term and not to the magnitude of D[44] and is not observed in X-band EPR. However, the sign of even a very small D can be determined from low-temperature HF EPR spectra.

There are many mathematical approaches applied for the analysis of the g-factors in low-spin d^5 systems.[45−49] In the treatment below, the simple and beautiful method presented by McGarvey was used.[50] The Kramer's doublet functions for the ground state for the complexes with C_2 symmetry are as follows:

$$\psi_+ = A|xy, \; 1/2> + B|xz, \; -1/2> + C|yz, \; -1/2>$$

$$\psi_- = -A|xy, \; -1/2> + B|xz, \; 1/2> - C|yz, \; 1/2>$$

The principal g values are then:

$$g_{xx} = 2[B^2 - A^2 - C^2 - 2kAC]$$

$$g_{yy} = 2[C^2 - B^2 - A^2 - 2kAB]$$

$$g_{zz} = 2[A^2 - C^2 - B^2 - 2kBC]$$

with k being the orbital reduction factor.

The symmetry of the cis-[Ru^{III}Cl$_2$(pic)$_2$]$^-$ ion is at best C$_2$, ignoring the small degree of nonequivalent Ru-X (X = N, O, Cl) bond distances and X−Ru−X angles. The z axis is defined as perpendicular to the RuCl$_2$O$_2$ "plane" and is very close to the N−Ru−N "direction". The x and y axes lay in the RuCl$_2$O$_2$ "plane" in such a way that x axis bisects two Ru−Cl bond (C$_2$ axis), while the y axis passes between two Ru−Cl and Ru−O bonds.

The wave function normalization coefficients and the orbital reduction factor were calculated from experimental g-factors using iterative procedure described by McGarvey.[51] Then, values of Δ/ζ and V/ξ (where Δ and V − axial and rhombic ligand field parameters, respectively, ξ − one electron spin−orbit coupling constant) were obtained (Table 4).

As we can see, both solutions presented in Table 4 give g-factors very close to the experimental values. However, they differ strongly in values of Δ/ξ and V/ξ. The latter probably cannot be considered as real due to structural aspects (see above). The former appears to be very likely and is consistent with the results for other strong-field low-spin d^5 ruthenium-(III) and iron(III) cis-MX$_4$Y$_2$ complexes with approximately C$_2$ symmetry for which a solution with higher absolute values of Δ and V are preferred.[50,52,53]

The zero-field splitting in this system must be caused by interactions between unpaired electrons on two Ru(III) moieties. Since an $S = 1$ state appears to be observed, the metal−metal interactions seem to occur in discrete pairs rather than involving more molecules. The closest Ru−Ru distance of 7.250 Å is found between the original Ru(III) moiety and the one generated by the symmetry operation $[2 - x, 1 - y, 1 - z]$. The Ru−Ru distance to a moiety generated by symmetry operation $[2 - x, 2 - y, 1 - z]$ is 8.699 Å, and in the latter case, the π−π stacking interactions are observed between two pyridine rings (see Figure 3). The magnitude of the D parameter, while very small, is still too large to be attributed to the dipole−dipole interactions between electrons localized on the Ru(III) ions at such distances. A possible explanation could be electron delocalization onto the pyridine rings, bringing some fraction of the two electronic densities in the configuration of Figure 3 closer to each other. Strengthening of the dipolar interactions due to electron delocalization has been reported.[54] This effect is, however, still insufficient in the present case, and presumably the anisotropic exchange must contribute to the zero-field splitting. The theory of the latter is complicated,[55] and to our knowledge it has never been applied to systems like ours. It should be mentioned here that there may be more metal−metal interactions in this system, where a given Ru(III) moiety engages in the hydrogen bonds with all its four neighbors (Figures S2, S3, and S4). The fact that a triplet-like spectrum is observed probably means that one of

Table 4. Solutions of g Equations for [Ru^{II}(bipy)$_2$(pic)]$^+$[cis-Ru^{III}Cl$_2$(pic)$_2$]$^-$ for Two Possible Sign Assignments

no.	g_{xx}	g_{yy}	g_{zz}	A	B	C	k	Δ/ξ	V/ξ
1	−2.532	−2.441	1.707	0.975	0.148	0.166	0.955	3.452	0.473
2	−2.536	−2.437	−1.703	0.647	0.532	0.546	1.183	0.266	0.040
exp	2.533	2.440	1.705						

the interactions is dominant and other ones do not cause additional zero-field splitting. The observed splitting could be due to weak isotropic exchange interactions between the Ru moieties with nonparallel axes of g. However, such a model predicts that the lower-field components of the $g = 2.533$ and of the $g = 1.705$ features should both be enhanced at the lowest temperatures or should both disappear, depending on the sign of the exchange constant. The pattern shown in Figures 12 and 13 is consistent with the presence of the D parameter, whatever its origin may be.

"Broken Symmetry" DFT Calculations. To gain insight into the possible exchange interactions between various Ru(III) moieties in our system, "broken symmetry" calculations[56−59] were performed. Each Ru moiety has four neighbors in the lattice. Hydrogen bonds to each of these neighbors are possible, and in addition, the $\pi-\pi$ interactions are possible in one case. In the "broken symmetry" method, two SCF calculations were performed: first, the spins on the interacting atoms were assumed parallel, and in the second calculation the spins were assumed antiparallel, which is referred to as a "broken symmetry state". The exchange constant, J, value was subsequently evaluated from the energy difference between the high-spin state and the broken symmetry state:

$$J = 2(E[HS] - E[BS])/(S_{max}*(S_{max} + 1))^{60}$$

The ORCA software package[61] was employed. Functional B3LYP was used with def2-TZVPP[62] functions for all atoms.[63−65] The ECP parameters for Ru [Def2-ECP] were obtained from TURBOMOLE (7.0.2).[62] These calculations produced very small antiferromagnetic J values (using the Heisenberg−Dirac Van Vleck Hamiltonian in the form $H = JS_1S_2$), of 0.38 and 0.50 cm^{-1} for the interactions involving only the H-bonds and −0.06 cm^{-1} (ferromagnetic) for the pair involved in the $\pi-\pi$ interactions (see Figures 3, S2−S4). Thus, the DFT calculations favor the interactions involving H-bonds to account for the observed exchange interactions between various Ru(III) centers in the lattice.

CONCLUSIONS

Our synthetic efforts have shown the way to prepare more such mixed-valence Ru(II)/Ru(III) ion-pairs that could in principle have interesting material properties for application as redox catalysts, antitumor complexes, and in redox cell biology. A challenge will be to synthesize other mixed-valence Ru(II)/Ru(III) ion-pairs with charge combinations of 2+/2−, 2+/1−, and 1+/2− for a variety of selected ligands and chelates. Although magnetic data and frozen solution EPR spectrum of $[Ru^{II}(bipy)_2(pic)]^+[cis\text{-}Ru^{III}Cl_2(pic)_2]^-$ are typical for $S = 1/2$, high-field EPR allowed us to prove that additional signals unexpected for d^5 systems are due to zero-field splitting caused by interactions between two neighboring Ru(III) ions, resulting in the $S = 1$ state.

ASSOCIATED CONTENT

Supporting Information

The Supporting Information is available free of charge at https://pubs.acs.org/doi/10.1021/acs.inorgchem.0c01068.

> X-ray structure of $[Ru^{II}(bipy)_2(pic)]Cl \cdot 5.5H_2$ and other experimental data for the mixed-valence ion-pair complex: additional structural information, SEM images, IR and ^1H NMR spectra, XRD analysis (PDF)

Accession Codes

CCDC 1857947 and 1909847 contain the supplementary crystallographic data for this paper. These data can be obtained free of charge via www.ccdc.cam.ac.uk/data_request/cif, or by emailing data_request@ccdc.cam.ac.uk, or by contacting The Cambridge Crystallographic Data Centre, 12 Union Road, Cambridge CB2 1EZ, UK; fax: +44 1223 336033.

AUTHOR INFORMATION

Corresponding Authors

Rudi van Eldik − *Faculty of Chemistry, Nicolaus Copernicus University in Toruń, 87-100 Toruń, Poland; Faculty of Chemistry, Jagiellonian University, 30-387 Kraków, Poland; Department of Chemistry and Pharmacy, University of Erlangen-Nuremberg, 91058 Erlangen, Germany;* orcid.org/0000-0003-4271-0118; Email: rudi.vaneldik@fau.de

Andrew Ozarowski − *National High Magnetic Field Laboratory, Tallahassee, Florida 32310, United States;* orcid.org/0000-0001-6225-9796; Email: ozarowsk@magnet.fsu.edu

Authors

Olga Impert − *Faculty of Chemistry, Nicolaus Copernicus University in Toruń, 87-100 Toruń, Poland*

Anna Kozakiewicz − *Faculty of Chemistry, Nicolaus Copernicus University in Toruń, 87-100 Toruń, Poland*

Grzegorz Wrzeszcz − *Faculty of Chemistry, Nicolaus Copernicus University in Toruń, 87-100 Toruń, Poland;* orcid.org/0000-0002-2132-2119

Anna Katafias − *Faculty of Chemistry, Nicolaus Copernicus University in Toruń, 87-100 Toruń, Poland;* orcid.org/0000-0001-5536-4280

Alina Bieńko − *Faculty of Chemistry, University of Wroclaw, 50-383 Wroclaw, Poland*

Complete contact information is available at:
https://pubs.acs.org/10.1021/acs.inorgchem.0c01068

Author Contributions

The synthetic work was done by O.I. The crystal structures were resolved by A.Ko. The EPR measurements were performed by G.W. and A.O. The experimental work was coordinated by A.Ka. A.B. performed the magnetic measurements and recorded the X-band EPR spectrum of a frozen solution of the ion-pair complex. A.O. performed the DFT calculations. R.v.E. and A.O. developed the concept of the manuscript and accept responsibility for the reported work. All authors contributed equally to writing the manuscript.

Notes

The authors declare no competing financial interest.

■ REFERENCES

(1) Browne, W. R.; Holder, A. A.; Lawrence, M. A.; Bullock, J. L., Jr.; Lilge, L., Eds.; *Ruthenium Complexes: Photochemical and Biomedical Applications*; Wiley-VCH Verlag GmbH & Co: Weinheim, 2018.

(2) Chang, W.; Lewis, A. R.; Prosser, K. E.; Thompson, J. R.; Gladkikh, M.; Bally, M. B.; Warren, J. J.; Walsby, Ch. J. CF_3 Derivatives of the anticancer Ru(III) complexes KP1019, NKP-1339, and their imidazole and pyridine analogues show enhanced lipophilicity, albumin interactions, and cytotoxicity. *Inorg. Chem.* 2016, *55*, 4850−4863.

(3) Lin, K.; Zhao, Z.-Z.; Bo, H.-B.; Hao, X.-J; Wang, J.-Q. Applications of ruthenium complex in tumor diagnosis and therapy. *Front. Pharmacol.* 2018, *9*, art. 1323.

(4) Zhang, P.; Sadler, P. J. Redox-active metal complexes for anticancer therapy. *Eur. J. Inorg. Chem.* 2017, 1541−1548.

(5) Alessio, E. Thirty years of the drug candidate NAMI-A and the myths in the field of ruthenium anticancer compounds: A personal perspective. *Eur. J. Inorg. Chem.* 2017, 1549−1560.

(6) Soldevila-Barreda, J. J.; Romero-Canelón, I.; Habtemariam, A.; Sadler, P. J. Transfer hydrogenation catalysis in cells as a new approach to anticancer drug design. *Nat. Commun.* 2015, *6*, 6582−6590.

(7) Ude, Z.; Romero-Canelon, I.; Twamley, B.; Fitzgerald Hughes, D.; Sadler, P. J.; Marmion, C. J. A novel dual-functioning ruthenium(II)−arene complex of an anti-microbial ciprofloxacin derivative — Anti-proliferative and anti-microbial activity. *J. Inorg. Biochem.* 2016, *160*, 210−217.

(8) Chen, F.; Soldevila-Barreda, J. J.; Romero-Canelón, I.; Coverdale, J. P. C.; Song, J.-I.; Clarkson, G. J.; Kasparkova, J.; Habtemariam, A.; Brabec, V.; Wolny, J. A.; Schünemann, V.; Sadler, P. J. Effect of sulfonamidoethylenediamine substituents in Ru^{II} arene anticancer catalysts on transfer hydrogenation of coenzyme NAD^+ by formate. *Dalton Trans.* 2018, *47*, 7178−7189.

(9) Gatti, A.; Habtemariam, A.; Romero-Canelon, I.; Song, J.-I.; Heer, B.; Clarkson, G. J.; Rogolino, D.; Sadler, P. J.; Carcelli, M. Half-sandwich arene ruthenium(II) and osmium(II) thiosemicarbazone complexes: solution behavior and antiproliferative activity. *Organometallics* 2018, *37*, 891−899.

(10) Chen, F.; Romero-Canelon, I.; Soldevila-Barreda, J. J.; Song, J.-I.; Coverdale, J. P. C.; Clarkson, G. J.; Kasparkova, J.; Habtemariam, A.; Wills, M.; Brabec, V.; Sadler, P. J. Transfer hydrogenation and antiproliferative activity of tethered half-sandwich organoruthenium catalysts. *Organometallics* 2018, *37*, 1555−1566.

(11) Katafias, A.; Impert, O.; Kita, P.; Fenska, J.; Koter, S.; Kaczmarek-Kędziera, A.; Różycki, H.; Bajek, A.; Uzarska, M.; van Eldik, R. Kinetics and mechanism of the reduction of *mer*-tris-picolinatoruthenium(III) by L-ascorbic acid. *Eur. J. Inorg. Chem.* 2014, 2529−2535.

(12) Impert, O.; Katafias, A.; Wrzeszcz, G.; Muzioł, T.; Hrynkiewicz, K.; Olejnik, N.; Chrzanowska, M.; van Eldik, R. Synthesis and detailed characterization of *cis*-dichloridobispicolinatoruthenate(III) as solid and in solution. *J. Coord. Chem.* 2016, *69*, 2107−2120.

(13) Impert, O.; Katafias, A.; Fenska, J.; Chrzanowska, M.; Koter, S.; Dücker-Benfer, C.; van Eldik, R. Mechanistic complications caused by redox equilibration: ascorbate reduction of a ruthenium(III) complex under low driving force conditions. *Eur. J. Inorg. Chem.* 2016, 5380−5386.

(14) Impert, O.; Katafias, A.; Chrzanowska, M.; Muzioł, T.; Wrzeszcz, G.; van Eldik, R. Redox equilibration observed for the reduction of a ruthenium(III) complex by ascorbate under low-driving-force conditions. *Eur. J. Inorg. Chem.* 2017, 3275−3284.

(15) Chrzanowska, M.; Katafias, A.; Impert, O.; Kozakiewicz, A.; Surdykowski, A.; Brzozowska, P.; Franke, A.; Zahl, A.; Puchta, R.; van Eldik, R. Structure and reactivity of [Ru^{II}(terpy)(N∧N)Cl]Cl complexes: consequences for biological applications. *Dalton Trans.* 2017, *46*, 10264−10280.

(16) Chrzanowska, M.; Katafias, A.; Kozakiewicz, A.; Puchta, R.; van Eldik, R. Systematic tuning of the reactivity of [Ru^{II}(terpy)(N∧N)-Cl]Cl complexes. *J. Coord. Chem.* 2018, *71*, 1761−1777.

(17) Tom, G. M.; Creutz, C.; Taube, H. Mixed valence complexes of ruthenium ammines with 4,4′-bipyridine as bridging ligand. *J. Am. Chem. Soc.* 1974, *96*, 7827−7829.

(18) Sutton, J. E.; Taube, H. Metal to metal interactions in weakly coupled mixed-valence complexes based on ruthenium ammines. *Inorg. Chem.* 1981, *20*, 3125−3134.

(19) (a) Kaim, W.; Lahiri, G. K. Unconventional Mixed-Valent Complexes of Ruthenium and Osmium. *Angew. Chem., Int. Ed.* 2007, *46*, 1778−1796. (b) Kaim, W. Concepts for metal complex chromophores absorbing in the near infrared. *Coord. Chem. Rev.* 2011, *255*, 2503−2513.

(20) (a) Li, F.; Collins, J. G.; Keene, F. R. Ruthenium complexes as antimicrobial agents. *Chem. Soc. Rev.* 2015, *44*, 2529−2542. (b) Hazari, A. S.; Indra, A.; Lahiri, G. K. Mixed valency in ligand-bridged diruthenium frameworks: divergences and perspectives. *RSC Adv.* 2018, *8*, 28895−28908. (c) Thomas, J. A. Tuning electronic interactions in mixed valence ruthenium systems incorporating thiacrown ligands. *Coord. Chem. Rev.* 2013, *257*, 1555−1563.

(21) Toyama, M.; Nakayasu, T.; Nagao, N. Crystal structure of (2-picolinato)bis(2,2′-bipyridine)ruthenium(II) chloride. *X-Ray Struct. Anal. Online* 2017, *33*, 11−13.

(22) Sullivan, B. P.; Salmon, D. J.; Meyer, T. J. Mixed phosphine 2,2′-bipyridine complexes of ruthenium. *Inorg. Chem.* 1978, *17*, 3334−3341.

(23) Figgis, N.; Nyholm, R. S. A convenient solid for calibration of the Gouy magnetic susceptibility apparatus. *J. Chem. Soc.* 1958, 4190−4191.

(24) Bain, G. A.; Berry, J. F. Diamagnetic corrections and Pascal's constants. *J. Chem. Educ.* 2008, *85*, 532−536.

(25) Ozarowski, A. *Doubletexact program*; NHMFL, Florida University: Tallahassee, USA.

(26) Hassan, A. K.; Pardi, L. A.; Krzystek, J.; Sienkiewicz, A.; Goy, P.; Rohrer, M.; Brunel, L. C. J. Ultrawide band multifrequency high-field EMR technique: A methodology for increasing spectroscopic information. *J. Magn. Reson.* 2000, *142*, 300−312.

(27) Sheldrick, G. M. Crystal structure refinement with *SHELXL*. *Acta Crystallogr., Sect. C: Struct. Chem.* 2015, *C71*, 3−8.

(28) *CrysAlis 171.38.43 package of programs*; Rigaku Oxford Diffraction, 2015.

(29) Groom, C. R.; Bruno, I. J.; Lightfoot, M. P.; Ward, S. C. The Cambridge Structural Database. *Acta Crystallogr., Sect. B: Struct. Sci., Cryst. Eng. Mater.* 2016, *B72*, 171−179.

(30) Canty, A. J.; Traill, P. R.; Skelton, B. W.; White, A. H. Alkene analogues of bis(N-donor)ketone ligands: ruthenium(II) complexes containing 1-(pyridin-2-yl)-1-(N-methylimidazol-2-yl)ethene and 1,1-bis(N-methylimidazol-2-yl)ethene (($mim)_2CCH_2$), and structural studies of [Ru(bpy)$_2${($mim)_2CCH_2$}][PF_6]$_2$ (bpy = 2,2′-bipyridine) and the pyridine-2-carboxylate ($pyCO_2^-$) complex [Ru-(bpy)$_2$($pyCO_2$)][PF_6]. *Inorg. Chim. Acta* 1997, *255*, 117−123.

(31) Yoshida, S.; Asai, M. Infrared spectra of pyrazine- and pyridine-carboxylic acid and their derivatives. *Chem. Pharm. Bull.* 1959, *7*, 162−171.

(32) Goher, M. A. S.; Abu-Youssef, M. A. M.; Mautner, F. A. Synthesis, spectral and structural characterization of a monomeric chloro complex of zinc(II) with picolinic acid, [Zn($C_5H_4NCO_2H$)-($C_5H_4NCO_2$)Cl]. *Polyhedron* 1996, *15*, 453−457.

(33) Ghatak, N.; Chakravarty, J.; Bhattacharya, S. Characterization and electron transfer properties of some picolinate complexes of ruthenium. *Polyhedron* 1995, *14*, 3591−3597.

(34) Impert, O.; Katafias, A.; Kita, P.; Wrzeszcz, G.; Fenska, J.; Lente, G.; Fabian, I. Base hydrolysis of mer-trispicolinatoruthenium-(III): kinetics and mechanism. *Transition Met. Chem.* 2011, *36*, 761−766.

(35) Nakamoto, K. *Infrared and Raman Spectra of Inorganic and Coordination Compounds, Part B*, 6th ed.; Wiley: New York, 2009.

(36) Deacon, G. B.; Phillips, R. J. Relationships between the carbon-oxygen stretching frequencies of carboxylato complexes and the type of carboxylate coordination. *Coord. Chem. Rev.* **1980**, *33*, 227−250.

(37) Xie, Y.-F.; Zhu, H.; Shi, H.-T.; Jia, A.-Q.; Zhang, Q.-F. Ruthenium complexes containing pyridine-2,6-dicarboxylato ligands. *Inorg. Chim. Acta* **2015**, *428*, 147−153.

(38) Kirillov, A. M.; Haukka, M.; Guedes da Silva, M. F. C.; Pombeiro, A. J. L. Synthesis, characterization and redox behaviour of mono- and dicarbonyl phosphane rhenium(I) complexes bearing N-, N,N- and N,O-type ligands. *Eur. J. Inorg. Chem.* **2007**, 1556−1565.

(39) http://www.sisweb.com/mstools/isotope.htm.

(40) Norrby, T.; Borje, A.; Akermark, B.; Hammarstrom, L.; Alsins, J.; Lashgari, K.; Norrestam, R.; Martensson, J.; Stenhagen, G. Synthesis, structure, and photophysical properties of novel ruthenium-(II) carboxypyridine type complexes. *Inorg. Chem.* **1997**, *36*, 5850−5858.

(41) Chilton, N. F.; Anderson, R. P.; Turner, L. D.; Soncini, A.; Murray, K. S. PHI: A Powerful New Program for the Analysis of Anisotropic Monomeric and Exchange-Coupled Polynuclear d- and f-Block Complexes. *J. Comput. Chem.* **2013**, *34*, 1164−1175.

(42) Sukanya, D.; Prabhakaran, R.; Natarajan, K. Ruthenium(III) complexes of dipicolinic acid with PPh3/AsPh3 as co-ligand: Synthesis and structural characterization. *Polyhedron* **2006**, *25*, 2223−2228.

(43) Dinelli, L. R.; Batista, A. A.; Wohnrath, K.; de Araujo, M. P.; Queiroz, S. L.; Bonfadini, M. R.; Oliva, G.; Nascimento, O. R.; Cyr, P. W.; MacFarlane, K. S.; James, B. R. Synthesis and characterization of [RuCl3(P-P)(H2O)] complexes; P-P = achiral or chiral, chelating ditertiary phosphine ligands. *Inorg. Chem.* **1999**, *38*, 5341−5345.

(44) Ozarowski, A. The zero-field-splitting parameter D in binuclear copper(II) carboxylates is negative. *Inorg. Chem.* **2008**, *47* (21), 9760−9762.

(45) Griffith, J. S. Theory of EPR in low-spin ferric haemoproteins. *Mol. Phys.* **1971**, *21*, 135−139.

(46) Hill, N. J. Electron paramagnetic resonance of osmium-doped trichlorotris(diethylphenylphosphine)rhodium(III). *J. Chem. Soc., Faraday Trans. 2* **1972**, *68*, 427−434.

(47) Taylor, C. P. S. The EPR of low spin heme complexes relation of the τ_{2g} hole model to the directional properties of the g tensor, and a new method for calculating the ligand field parameters. *Biochim. Biophys. Acta, Protein Struct.* **1977**, *491*, 137−149.

(48) Lahiri, G. K.; Bhattacharya, S.; Ghosh, B. K.; Chakravorty, A. Ruthenium and osmium complexes of N,O chelators: Syntheses, oxidation levels, and distortion parameters. *Inorg. Chem.* **1987**, *26*, 4324−4331.

(49) LaChance-Galang, K. J.; Doan, P.; Clarke, M. J.; Rao, U.; Yamano, A.; Hoffman, B. M. EPR and NMR spectra as probes of spin-density distribution in heterocyclic ligands coordinated in *trans*-[L(Im)(NH3)4Ru^{III}]: Implications for long-range electron transfer. Crystal structure of *trans*-[(Im)2(NH3)4Ru]Cl3·H2O. *J. Am. Chem. Soc.* **1995**, *117*, 3529−3538.

(50) McGarvey, B. R. Survey of ligand field parameters of strong field d^5 complexes obtained from the g matrix. *Coord. Chem. Rev.* **1998**, *170*, 75−92.

(51) McGarvey, B. R. ESR g matrix for strong field d^5 systems. *Quim. Nova* **1998**, *21*, 206−213.

(52) Hudson, A.; Kennedy, M. J. An electron resonance study of some low-spin d^5 complexes of second- and third-row transition metals. *J. Chem. Soc. A* **1969**, 1116−1120.

(53) Reiff, W.; DeSimone, R. E. Electronic ground states of dicyanobis(diimine)iron(III) compounds. *Inorg. Chem.* **1973**, *12*, 1793−1796.

(54) Riplinger, C.; Kao, J. P. Y.; Rosen, G. M.; Kathirvelu, V.; Eaton, G. R.; Eaton, S. S.; Kutateladze, A.; Neese, F. Interaction of radical pairs through-bond and through-space: Scope and limitations of the point−dipole approximation in electron paramagnetic resonance spectroscopy. *J. Am. Chem. Soc.* **2009**, *131*, 10092−10106.

(55) Maurice, R.; Sivalingam, K.; Ganyushin, D.; Guihéry, N.; de Graaf, C.; Neese, F. Theoretical determination of the zero-field splitting in copper acetate monohydrate. *Inorg. Chem.* **2011**, *50*, 6229−6236.

(56) Noodleman, L. Valence Bond Description of Antiferromagnetic Coupling in Transition Metal Dimers. *J. Chem. Phys.* **1981**, *74*, 5737−5743.

(57) Noodleman, L.; Davidson, E. R. Ligand Spin Polarization and Antiferromagnetic Coupling in Transition Metal Dimers. *Chem. Phys.* **1986**, *109*, 131−143.

(58) Malrieu, J. P.; Caballol, R.; Calzado, C. J.; de Graaf, C.; Guihéry, N. Magnetic Interactions in Molecules and Highly Correlated Materials: Physical Content, Analytical Derivation, and Rigorous Extraction of Magnetic Hamiltonians. *Chem. Rev.* **2014**, *114*, 429−492.

(59) Rodríguez-Fortea, A.; Alemany, P.; Alvarez, S.; Ruiz, E. Exchange Coupling in Halo-Bridged Dinuclear Cu(II) Compounds: A Density Functional Study. *Inorg. Chem.* **2002**, *41*, 3769−3778.

(60) Bencini, A.; Gatteschi, D. Xa-SW Calculations of the Electronic Structure and Magnetic Properties of Weakly Coupled Transition-Metal Clusters. The [Cu2Cl6]$^{2-}$ Dimers. *J. Am. Chem. Soc.* **1986**, *108*, 5763−5771.

(61) Neese, F. *ORCA − An Ab Initio, Density Functional and Semiempirical Program Package*, Version 4.0.1; Surf Sara: Amsterdam, 2017. Neese, F. The ORCA Program System. The ORCA program system*Wiley Interdiscip. Rev.: Comput. Mol. Sci.* **2012**, *2*, 73−78

(62) (a) Weigend, F.; Ahlrichs, R. Balanced basis sets of split valence, triple zeta valence and quadruple zeta valence quality for H to Rn: Design and assessment of accuracy. *Phys. Chem. Chem. Phys.* **2005**, *7*, 3297. (b) Andrae, D.; Haeussermann, U.; Dolg, M.; Stoll, H.; Preuss, H. Energy-Adjusted ab-initio Pseudopotentials for the 2nd and 3rd Row Transition Elements. *Theor. Chim. Acta* **1990**, *77*, 123−141. (c) Furche, F.; Ahlrichs, R.; Hattig, C.; Klopper, W.; Sierka, M.; Weigend, F. Turbomole. *Wiley Interdiscip. Rev.: Comput. Mol. Sci.* **2014**, *4*, 91−100.

(63) Schäfer, A.; Horn, H.; Ahlrichs, R. Fully Optimized Contracted Gaussian Basis Sets for Atoms Li to Kr. *J. Chem. Phys.* **1992**, *97*, 2571−2577.

(64) The Ahlrichs auxiliary basis sets (https://www.basissetexchange.org/) have been hardwired into the ORCA software.

(65) Eichkorn, K.; Weigend, F.; Treutler, O.; Ahlrichs, R. Auxiliary Basis Sets for Main Row Atoms and Transition Metals and Their Use to Approximate Coulomb Potentials. *Theor. Chem. Acc.* **1997**, *97*, 119−124.